JOURNAL OF SOLID STATE CHEMISTRY 6, 352–364 (1973)

Molecular Orbital Description of the Metal–Semiconductor Interface of Ag–AgBr

R. C. BAETZOLD

Research Laboratories, Eastman Kodak Company, Rochester, New York 14650

Received May 3, 1972

Extended Hückel (EH) and CNDO methods are applied to a cluster (up to 35 ions) of an ionic semiconductor (AgBr) and its interface with a metal (Ag). It is shown that EH suitably modified to include charge and Madelung effects and CNDO provide a suitable treatment for these systems. Comparison of calculated AgBr data with experimental data shows 10–20% agreement. Significant electron transfer from silver atoms to silver bromide takes place, but as the silver cluster is made larger the average charge transferred decreases. Calculated data for this system lead to a thermodynamic pathway for the photochemical decomposition of AgBr involving electron capture by odd-size silver centers and silver ion capture by even-size silver centers.

Introduction

The object of this report is twofold. First, the electronic characteristics of the metal–semiconductor interface Ag–AgBr will be described. The second purpose is to show the degree to which extended Hückel (EH), suitably modified to include charge and Madelung effects, and complete neglect of differential overlap (CNDO) calculation models are capable of treating ionic solids and their interactions with adsorbates. Comparison of results from the two methods shows that many calculated electronic properties and trends agree with the experimental. Some properties are calculated more accurately by one of the methods than by the other; the reliability and limitations of these procedures for solid-state problems are discussed.

It is by no means a foregone conclusion that molecular-orbital methods of calculation can give an accurate picture of binding in ionic–solid materials. The success that semiempirical methods have had for molecular systems suggests that they should be applied to crystals to see whether the results are reliable. The approximations involved in applying these methods to ionic crystals are numerous. Included in these are the approximate nature of the calculation which makes it uncertain whether high atomic number elements or ionic systems can be treated. In addition, a small number of atoms are used to represent the bulk crystal. Earlier results (*1*) have shown that the picture of binding in some high atomic number elements like Ag is reasonable. Hayns (*2a*) has successfully treated LiF by CNDO and concludes that the approach is useful in crystalline solids. The EH method has recently been applied to Tl impurity levels in KCl to give a consistent interpretation of the absorption spectrum (*2b*). Other recent work applying semiempirical methods to solids includes a calculation of impurity levels in diamond (*3a*), chemisorption on graphite (*3b,c*) and hydrogen adsorption on nickel crystal (*3d*). In light of these results, there is reason to expect a degree of success in treating Ag clusters on AgBr.

The basic calculational techniques have been described by Hoffmann (*4*) and Pople and coworkers (*5*). To treat the ionic solids by EH we have applied the methods described by Cusachs (*6*) for ionic diatomic species. The basic effects of charge on energy levels has also been described by Brown (*7*) in terms of ionization effects and Madelung effects. These effects must be included in calculations for ionic crystals as our data shows.

Method of Calculation

The EH (*4*) and CNDO (*5*) procedures have been applied to the Ag–AgBr interface problem.

The former technique has required modification to take into account charge effects in ionic crystals. The CNDO procedure is well suited for this type of calculation since the Hamiltonian matrix elements are explicitly dependent on the charge distribution in the molecule. In EH only the 5*s* orbitals of Ag and 4*p* orbitals of Br were used in forming wavefunctions. In CNDO it was necessary to include the next set of unfilled atomic orbitals on each atom.

Modifications to EH

The necessary effects to account for in calculations for ionic systems by EH have been discussed (*6*). We have employed the procedure used by Cusachs in calculation for diatomic molecules. The application of this technique to crystals has involved the use of Madelung-type summations. These features are described for an atomic orbital *i* located on atom A with charge q_A.

The valence-state ionization potential (VSIP) is a function of charge on the atom (q_A). A linear dependence is assumed, although more complicated functions could be used. The diagonal Hamiltonian matrix element is given by

$$\mathscr{H}_{ii} = -\mathrm{IP} = -A_i - B_i q_A. \tag{1}$$

The ionization potential of the *i*th orbital on the neutral atom is A_i, and the linear factor B_i of the lowest unfilled atomic level is calculated from the electron affinity (EA) by

$$B_i = \mathrm{IP}_i - \mathrm{EA}_i. \tag{2}$$

In other cases B_i can be obtained from spectroscopic data on the ionized species.

Atomic ionization potentials are changed by the charges of adjacent atoms. Thus, the matrix elements are

$$\mathscr{H}_{ii} = -A_i - B_i q_A - \sum_{B \neq A} V(R_{AB}), \tag{3}$$

where $V(R_{AB})$ is the potential at A caused by the change q_B, a distance R_{AB} away. The potential terms have been evaluated as coulomb terms in the past (*8*),

$$V(R_{AB}) = q_B e^2 / R_{AB}, \tag{4}$$

or by the quantum mechanical expressions employed by Cusachs (*6*),

$$V(R_{AB}) = (B_i/0.73)\left\{Z_B F_0(R_{AB}/r_A) + \sum_{B \neq A} q_B F_0(r_B/F_0(R_{AB}/r_B)r_A)\right\}, \tag{5}$$

where $r_A^{-1} = \int \phi_i(1/r)\phi_i d_j$, $F_0(x) = (1-(1+x)\text{-}e^{-2x})/x$, Z_B = number of valence electrons on atom B, and q_B = charge due to valence electrons on atom B.

The quantum mechanical expression is used to evaluate $V(R_{AB})$ for each pairwise interaction in the present model. A simplification resulting in convergence for fewer iterations is achieved by keeping $\mathscr{H}_{ii}$ values of the AgBr lattice constant and only varying $\mathscr{H}_{ii}$ of the adsorbed Ag atoms. The $\mathscr{H}_{ii}$ values chosen for AgBr are determined by the $\mathscr{H}_{ii}$ values obtained upon convergence of the isolated AgBr lattice. In this way, only effects of the lattice on the adsorbed atoms are included and this is referred to as a type I calculation. Type II calculations include the full $V(R_{AB})$ terms. The noniterative version of EH in which only the A_i term of Eq. (1) is nonzero will be referred to as a type III calculation.

Both EH and CNDO techniques employed require iteration to get a self-consistent result. Several cycles are usually required for convergence to within a charge on each atom of 0.02 e.u. Convergence problems in CNDO were eliminated by using a type of averaged output–input charge (*3b*). The input P_{kj} for a new cycle was taken as

$$P_{kj} = \delta P_{kj}^{\,o} + (1-\delta)P_{kj}^{\,i}, \tag{6}$$

where the superscripts *o* and *i* denote output and input of the previous cycle and P_{kj} is a bond–density matrix element. A value of 0.1 to 0.3 for δ was sufficient to give convergence for the most difficult cases.

The parameters used in this work are listed in Table I. Ionization potential data (A_i) come from atomic spectroscopic tables (*9*). Electron

TABLE I

PARAMETERS USED IN CALCULATIONS

Element	β°	CNDO Orbital	½ (IP + EA)	α
Ag	−2	5*s*	4.26	1.35
		5*p*	2.39	1.35
Br	−5	4*p*	7.61	2.26
		5*s*	2.30	2.26

Element	EH Orbital	A_i	B_i	α
Ag	5*s*	7.56	6.61	1.35
Br	4*p*	11.84	8.40	2.26

affinity data (*10*, *11*) are used to calculate B_i using Eq. (2). Estimates of EA have been used for the unoccupied orbitals used in the CNDO calculations. Screening parameters for the Slater orbitals are taken from Clementi et al. (*12*). The calculated atom charges (q) are determined by Mulliken analysis (*13*) for CNDO and EH calculations. The resonance parameter β^0 used in CNDO is chosen by fitting calculated data to experimental data for homonuclear diatomic molecules of the element in question. This procedure does not always give good fit for the heteronuclear diatomic as evidenced for the AgBr molecule where the calculated binding energy is 4.7 eV and the calculated energy of transition from ground to excited state is 5.4 eV. Experimental values for these quantities are 3.0 eV (*10*) and 3.9 eV (*14*), respectively. Binding energy is calculated as the difference in energy between the bonded configuration of atoms and the isolated atoms. In EH type calculations the splitting parameter $K = 1.75$ was employed as in other calculations of this type (*4*).

AgBr

Information concerning the band structure of silver halides has come from theoretical (*15*) and experimental (*7*, *16*, *17*) sources. Tight binding calculations reported have been done for a periodic lattice; they do not apply to surfaces. A significant feature of these calculations is the inverted valence-band structure which is responsible for a smaller indirect than direct band gap. This feature is explained by the mixing of halogen p orbitals and silver $4d$ orbitals. The calculated ionization potential of AgBr is nearly one R_y (−13.6 eV), which is quite different from the experimental value, ~6.5 eV.

The first concern in our calculations was whether the molecular-orbital techniques were a reasonable model for silver halide. The computer limits our calculations to no more than ~35 atoms, so the model is by no means periodic. On the other hand, the discontinuities present should give results more appropriate to surfaces. The crystal models treated are shown in Fig. 1. A rigid lattice with bulk experimental bond length 2.885 Å is assumed in this model. The model neglects lattice relaxations that occur in AgBr. This effect will be investigated in the future. A potential energy minimum within 0.1 of 2.885 Å occurs in CNDO, but no minimum is found in EH.

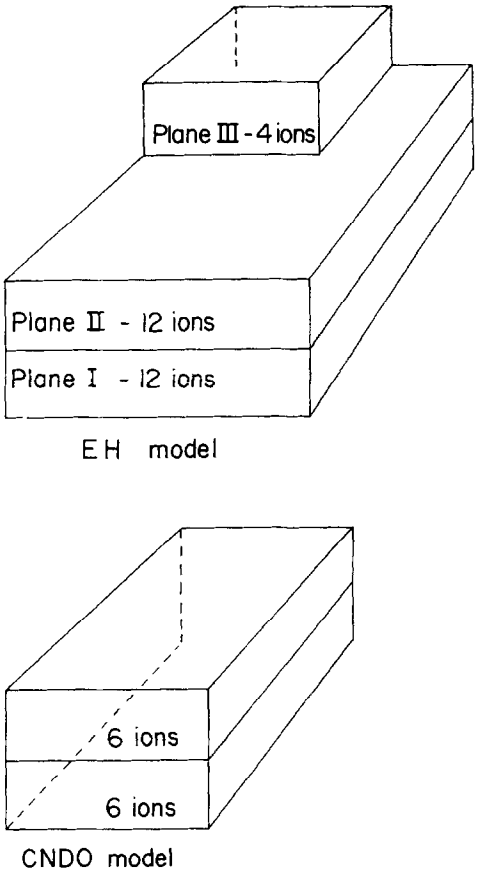

FIG. 1. Crystal models used in calculations.

CNDO

The crystal models of AgBr treated by CNDO have been small cubes or rectangular arrays. Orbitals used have been $5s$ and $5p$ on silver with or without the $4d$ orbitals; $4p$ and $5s$ have been used for Br. Density-of-states curves are shown in Fig. 2 for three different choices of the atomic parameter in the exponent of Slater $4d$ orbitals:

a. $\alpha = 2.19$, predicted by Slater's rules;

b. $\alpha = 3.61$, calculated by Hartree–Fock atomic calculations (*12*);

c. $\alpha = 1.91$, $n = 2$, $l = 2$, as described by Cusachs' matching overlap techniques (*18*).

In all cases, the d band is very narrow (0.3 eV for the first case) and for the first two cases is about 4 eV below the top of the valence band, in accord with recent experiments (*19*). The next higher energy states are halogen $4p$ states with

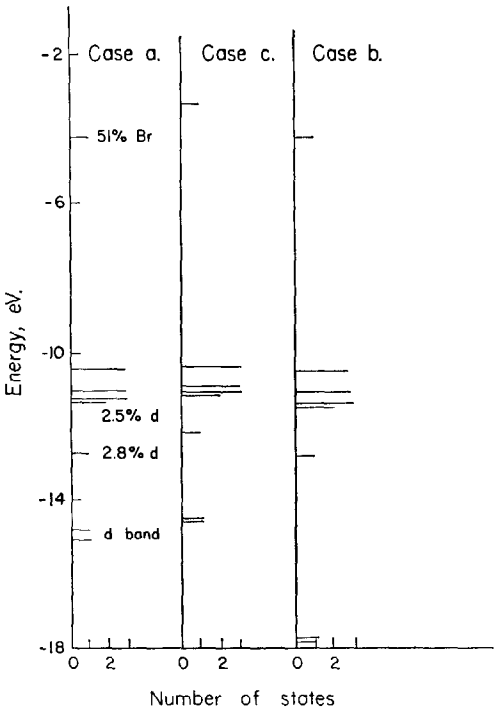

FIG. 2. Density of states for AgBr [CNDO] (percentages of orbitals in a particular wavefunction noted).

various mixtures of 5*s* silver orbitals. The lowest of these states contains a large contribution from silver orbitals, but the others are >99% halogen 4*p* states. Some 4*d* character is mixed with the halogen 4*p* states, as noted in Fig. 2. The lowest unoccupied state is separated by a large gap from the top of the valence band. This state contains a large number of 4*p* halogen orbitals along with 5*s* silver orbitals. The next higher state is analogous to a conduction-band state in that it is composed of 5*s* orbitals delocalized throughout the model.

The gap between HOMO and LUMO calculated by CNDO is a measure of semiconductor band gaps. This measure may be misleading because the position of each level calculated in CNDO depends upon the electron distribution. Excitation of an electron lowers the level receiving the electron and raises the level losing the electron. A value of the band gap closer to experimental values is found by comparing the energy of the ground and excited states as shown in Table II:

$$\Delta E_1 = E_{ex} - E_{gr}. \tag{7}$$

The experimental direct band gap is 4.29 eV in AgBr (*20*). In this table we have shown the effect of basis orbitals and crystal geometry on calculated properties. Geometry has little effect, but 4*d* orbitals have a big effect. The calculated binding energy per AgBr pair relative to atoms is much closer to the experimental (8.4 eV) (*7*) if 4*d* orbitals are not included. The electron affinity (EA) calculated by $EA = E_{gr} - E_{anion}$ comes closer to experimental values (3.9 eV) (*7*) if larger models are used. This seems reasonable since more charge delocalization can take place in larger models.

EH

The geometric models for AgBr contain up to 35 atoms in the EH procedure. The calculated data are shown for representative models in Table III. Comparison with CNDO indicates a much smaller gap and binding energy in EH. Apparently the type of coulombic interactions

TABLE II

CALCULATED AgBr DATA [CNDO]

Geometry	Orbitals used	BE/AgBr (eV)	HOMO (eV)	LUMO (eV)	ΔE_1 (eV)	EA (eV)
Cube	Ag: 4*d*, 5*s*, 5*p* Br: 4*p*, 5*s*	1.14	9.87	2.32	—	—
Cube	Ag: 5*s*, 5*p* Br: 4*p*, 5*s*	6.57	10.02	3.19	4.47	2.17
$(AgBr)_6$	Ag: 5*s*, 5*p* Br: 4*p*, 5*s*	6.70	9.88	3.85	4.22	3.14
$(AgBr)_8$	Ag: 5*s*, 5*p* Br: 4*p*, 5*s*	6.95	9.58	3.90	—	—

TABLE III

CALCULATED AgBr DATA [EH]

Model	Type calculated	BE/AgBr (eV)	HOMO (eV)	LUMO (eV)	ΔE^* (eV)
$(AgBr)_{16}$ 2 planes, periodic	II	1.29	10.83	10.03	2.60
$(AgBr)_{16}$ 2 planes, nonperiodic	II	0.93	10.87	10.09	2.29
$(AgBr)_{16}$ 2 planes, nonperiodic	III	5.30	11.67	10.06	3.26
$(AgBr)_{14}$ (Fig. 1)	II	0.71	10.24	9.70	1.72
$(AgBr)_8$ (like Fig. 1)	II	0.79	10.29	9.48	2.61

which contribute to the binding energy in AgBr are not treated fully by the EH calculation procedure. The nature of the band gap will be discussed, but a fundamental difference with CNDO is the insensitivity of positions of energy levels to electron occupancy in EH.

A density-of-states curve in Fig. 3 shows the semiconductor nature of AgBr. The states in the valence band are composed almost exclusively of halogen 4*p* states except for the lowest state, which (as in CNDO) contains significant contributions from 5*s* silver orbitals. The LUMO consists of halogen *p* orbitals pointing in each direction in which there is a missing bond and 5*s* silver orbitals in about equal proportion. Only one such state is found independent of AgBr model size. States above LUMO contain delocalized silver orbitals and are identifiable with the conduction band. Thus the band gap more appropriate to comparison with experimental information is taken between HOMO and the second excited state (ΔE^*).

In order to determine whether periodicity would change the band structure of AgBr, we have done calculations for a three-dimensional sheet infinite in two dimensions. This is done by replacing long-range interactions by short-range interactions (overlaps) for edge and corner atoms using a technique similar to that used to achieve periodicity in the graphite lattice (*3b*). The example for a 4 × 4 plane of AgBr in Fig. 4 illustrates this concept. Bonds between edge atoms with hypothetical nearest neighbor atoms (dotted lines) which would be present in an infinite sheet are simulated by modifying the overlap matrix. Long-range overlap elements involving orbitals from atoms on edges are replaced by nearest-neighbor overlap elements. The data in Table III show that this does not change the positions of energy levels significantly and has only a minor effect on the density of states. A significant decrease in the contributions of surface halogen *p* orbitals to LUMO is observed. The EH model of AgBr apparently contains discontinuity effects caused only by the large surface-to-volume ratio in this model.

The overall effect of ionicity is to decrease the difference between atomic ionization potentials

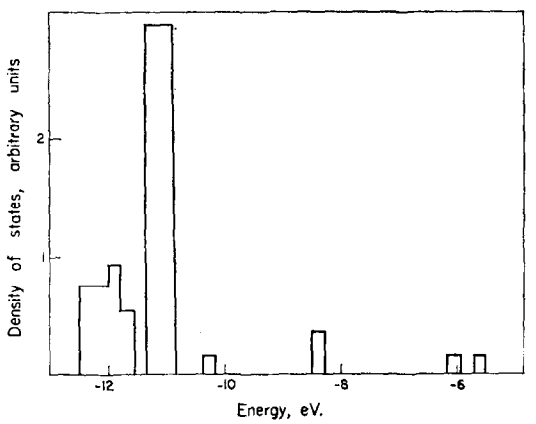

FIG. 3. Density of states for AgBr [EH].

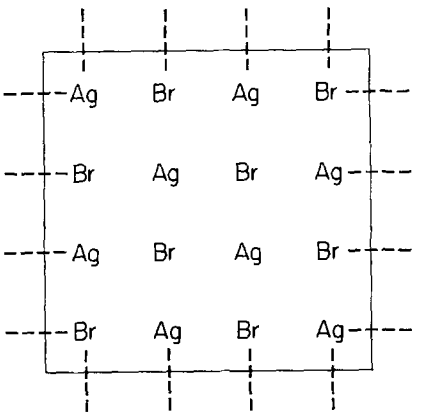

FIG. 4. Illustration of method of introducing periodicity in EH calculations.

of Ag and Br. This effect may be seen by evaluating the Madelung terms. We assume that

$$|Q_{Ag}| = |Q_{Br}| \tag{8}$$

for all lattice ions, and replace $\sum_{B\neq A} V(R_{AB})$ by a Madelung-type sum of the form

$$-3V(R_1) + 3V(R_1/\sqrt{2}) - V(R_1/\sqrt{3}) \ldots, \tag{9}$$

where R_1 is the nearest-neighbor distance of the crystal lattice. Applying Eq. (5) to calculate the $V(R_{AB})$ terms, we find that

$$-\mathscr{H}_{ii}^{Ag} = 7.56 + 0.84\, Q_{Ag},$$

and

$$-\mathscr{H}_{ii}^{Br} = 11.84 + 1.75\, Q_{Br}, \tag{10}$$

which means that the atomic levels converge as the crystal increases in ionicity.

Interface

Charge transfer at the Ag–AgBr interface is determined by the relative position of the Fermi levels in each material. In bulk Ag this level corresponds to the work function (4.5 eV). In AgBr the Fermi level is taken at the midpoint of the valence and conduction bands (Fig. 5) as appropriate for an intrinsic semiconductor. Thus, electrons would flow to AgBr if vacant energy levels below 4.5 eV are available. Movement of interstitial Ag^+ to Ag would accomplish a similar charge transfer. This direction of charge transfer is found in the molecular orbital calculations.

CNDO Results

Calculations at limited numbers of positions for Ag adsorption on the 12-ion AgBr model of Fig. 1 reveal that the most favorable position is directly over an interstitial site and not a lattice site,

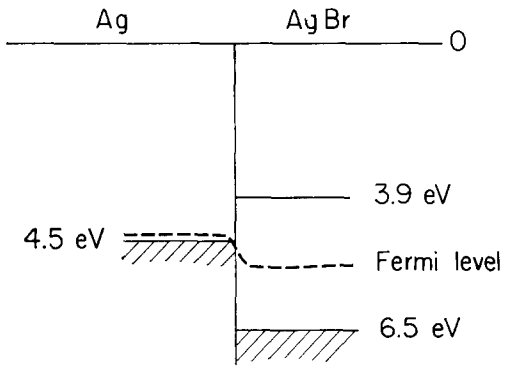

FIG. 5. Bulk Ag–AgBr interface.

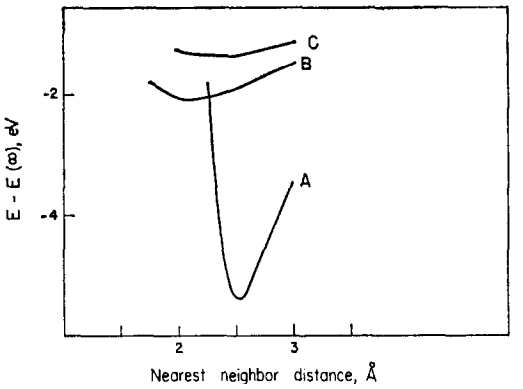

FIG. 6. Adsorption of Ag to $(AgBr)_6$ [CNDO]. Curve A: Ag in center of lattice site; Curve B: Ag over Ag ion; Curve C: Ag over Br ion.

as shown in Fig. 6. In addition, silver atoms are more stable over Ag ions than Br ions.

When the silver aggregate grows its properties become more like those of bulk silver. These calculations for Ag atoms added at lattice positions show that a single atom on the crystal has a charge of +0.52, which is comparable to the average AgBr lattice cation charge of +0.55 calculated by Mulliken analysis. Figure 7 shows the average charge on a silver aggregate in contact with AgBr as a function of size. The average charge decreases as size increases such that for Ag_6 the total positive charge is +0.65, which corresponds roughly to Ag_6^+. The probabilities of electron or hole capture by the silver aggregate are also indicated by this figure and were obtained by performing the Mulliken analysis on the

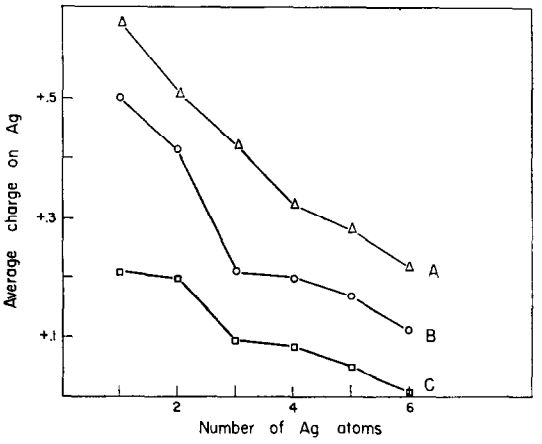

FIG. 7. Average charge on silver atoms vs number of silver atoms added to $(AgBr)_6$ [CNDO]. Curve A: system has one net positive charge; Curve B: neutral system; Curve C: system has one net negative charge.

LUMO and HOMO, respectively. The probability for electron or hole capture on the silver center increases with its size and becomes ~65% at six atoms.

The properties of the system silver atoms–silver halide matrix are displayed in Table IV. In this table, binding energy is the difference in energy E:

$$E_{(\text{lattice}+\text{Ag}_n)} - E_{\text{lattice}} - nE_{\text{Ag}}. \quad (11)$$

Ionization potentials are reported as Koopmans' theorem (HOMO) or the difference in energy:

$$\text{IP} = E_{\text{cation}} - E_{\text{neutral}}. \quad (12)$$

The electron affinity is given by LUMO or the difference in energy:

$$\text{EA} = E_{\text{neutral}} - E_{\text{anion}}. \quad (13)$$

Interaction of small neutral Ag particles and the AgBr lattice causes a reduction in energy. This is indicated by comparing binding energy for the silver aggregate isolated and in contact with the AgBr. The binding energy per atom becomes near constant at a few silver atoms. This behavior is unlike that calculated for isolated silver aggregates, where binding energy changes even when ten or more atoms are present.

The properties of charged particles of Ag on $(AgBr)_6$ in Tables IV and V show that the lattice affords a lowering of energy relative to isolated particles. Cationic particles increase in stability with size, but anionic particles show the reverse trend. The HOMO and LUMO are significantly shifted by the excess charge of the system.

The odd–even oscillation in HOMO and LUMO observed for silver aggregates is observed when AgBr crystal lattice is present. In addition, a linear relation exists between the ionization potential as calculated by the two approaches; the same is true of the electron affinity. As size increases, HOMO and LUMO tend generally to converge. This behavior is also present in isolated silver particles.

These data apply to silver atom formation on the surface of silver halide. We should like to point out that the electron-trapping ability of the two-atom silver center on AgBr is very poor. The electron affinity, as measured by either technique described above (LUMO or EA), of this center is less than the electron affinity of the crystal with no silver. Thus, growth of the silver center beyond this size must first occur by an ionic event; then an electron may be trapped. Calculations for isolated Ag_2^- indicate that it is

TABLE IV

SILVER PARTICLES ON $(AgBr)_6$

	CNDO				
Number of Ag centers	BE/atom (eV)	HOMO (eV)	LUMO (eV)	IP (eV)	EA (eV)
	Neutral Particles				
0	—	9.88	3.85	9.54	3.14
1	1.97	5.83	5.83	6.53	4.85
2	3.50	8.08	3.42	9.55	2.58
3	3.29	5.66	5.66	6.47	4.76
4	3.81	7.83	3.89	8.51	3.05
5	3.35	5.51	5.51	6.09	—
6	3.32	6.03	4.95	—	—
	Anionic particles				
0	—	2.11			
1	6.82	4.29			
2	4.80	1.86			
3	4.87	4.15			
4	4.37	2.30			
	Cationic particles				
0	—	11.94	11.94		
1	1.53	12.36	7.37		
2	1.78	10.36	10.36		
3	3.16	12.06	7.31		
4	3.00	9.42	9.42		
5	3.35	11.36	7.04		

TABLE V

ISOLATED SILVER PARTICLES

Number of Ag atoms	CNDO BE/atom (eV)	HOMO (eV)	LUMO (eV)	IP (eV)	EA (eV)
		Neutral particles			
1	0	—	—	—	—
2	2.96	8.10	0.35	10.39	1.38
3	1.73	4.24	4.24	5.39	3.24
4	2.39	6.78	2.06	7.95	0.89
5	3.54	3.87	3.87	5.16	2.85
6	3.71	5.99	1.43	7.31	0
		Anionic particles			
1	—	—	—	—	—
2	2.65	0	—	—	—
3	2.78	2.00	—	—	—
4	2.59	0	—	—	—
5	3.91	1.85	—	—	—
6	2.75	0	—	—	—
		Cationic particles			
1	—	—	—	—	—
2	1.48	12.07	—	—	—
3	1.97	13.33	—	—	—
4	0.38	9.08	—	—	—
5	2.30	11.84	—	—	—
6	2.50	8.33	—	—	—

unstable. Since the EA of even-size Ag aggregates increases with size, electrons could be trapped at those larger aggregates.

The gap between HOMO and LUMO of the neutral species can be taken as a measure of the energy of the first electronic transition. The trend of the data in Table IV is to decrease this gap as the number of silver particles increases, as was found for isolated silver particles. This effect is observed experimentally (*21*).

The effect of substrate on silver geometry is examined for a triatomic aggregate in Table VI. In the absence of substrate, the linear is the most stable form of silver, but these data show that a right triangle is more stable on AgBr. In these calculations all atoms were located at lattice sites 2.885 Å above the 12-ion AgBr model surface.

Calculations to examine the effect of AgBr substrate size on Ag_2 are displayed in Table VII. These data indicate that while the behavior of AgBr in CNDO depends upon lattice size, there is no saturation of the lattice by electron donation from Ag, since $(AgBr)_6$ accepts more electrons from Ag_2 than does $(AgBr)_8$. The variations in total binding energy may be spurious since convergence to only 0.03 e.u. was obtained for the larger model.

Polaron effects in AgBr can be examined by analysis of the changes in wavefunction caused by electron or hole addition to the system. An overlap population between atoms A and B is defined by

$$Q_{AB} = \sum_{\mu}^{A} \sum_{\nu}^{B} P_{\mu\nu} S_{\mu\nu}, \tag{14}$$

where $S_{\mu\nu}$ is an element of the overlap matrix and $P_{\mu\nu}$ is an element of the bond–density matrix calculated from the eigenvectors by (*5*)

$$P_{\mu\nu} = 2 \sum_{i=1}^{occ} C_{i\mu} C_{i\nu}. \tag{15}$$

The overlap population is a measure of the strength of the bond between A and B and is expected to be reciprocally related to bond length. It takes the average values 0.193, 0.187, and 0.168 for anionic, neutral, and cationic models, respectively. Thus, bond lengths de-

TABLE VI

GEOMETRY EFFECT

Geometry	BE (eV)	Average Ag charge	HOMO (eV)
90° triangle over 1 Br, 2 Ag	8.54	+0.26	5.26
90° triangle over 1 Ag, 2 Br	9.86	+0.24	5.66
Linear over 2 Br, 1 Ag	9.09	+0.24	5.88
Linear over 1 Br, 2 Ag	8.59	+0.21	5.83

crease in the presence of an excess electron and elongate in the presence of an excess hole. Using a harmonic potential, the polaron deformation energy is estimated to be 10 times greater for a hole than for an electron. High mobility is usually associated with low deformation energy in ionic crystals, so electrons would be expected to be more mobile than holes in AgBr. This is observed experimentally (*22*, *23*).

EH

Calculations have been performed for the model of Fig. 1 using the type I, II, and III EH procedures described earlier. Note that in this geometric model a defect feature resembling a kink site is present, since a new atom can occupy a lattice position with two nearest neighbors of the same charge. The prime advantage of EH over CNDO is the larger crystal model that can be treated.

The properties of Ag on AgBr calculated by the three EH procedures are shown in Table VIII. The binding energy is calculated from the difference in energy shown in Eq. (*11*). Here E_{lattice} is calculated for the same ionic situation as was observed when the silver interacted with the lattice. There is a stabilization of Ag on the lattice relative to the isolated silver particle. Stabilization results from electron transfer to the AgBr model. The binding energy per atom is near constant and independent of size in each of the three types of calculation. This behavior is unlike the increasing trend in BE/atom observed for isolated silver aggregates (*1*). The average charge on the silver aggregate is plotted versus size in Fig. 8 for the type II and III calculations. Note that the results of the type II calculation agree in form with CNDO results, although the silver particle has a lower charge in EH calculation. The type III calculation shows that silver is strongly ionized even at a size of a few atoms. This behavior is unrealistic based on stable aggregates of silver comprising four atoms, as observed photographically (*24*). The charges on the silver aggregate after adding a hole or an electron to the system indicate that neither of these particles is localized completely on the silver center. It is apparently the ionic and Madelung effects which result in localization of charge carriers on the silver aggregate.

The behavior of the HOMO and LUMO of $Ag_N(AgBr)_8$ is shown in Fig. 9 using the type II calculation. Note the general trend resulting in a decrease in IP and EA as the size of the silver aggregate increases. The trend in IP is in accord with that previously observed for isolated Ag aggregates and observed in CNDO. The reverse is true of the trend in LUMO, since in isolated particles EA increases as size increases. This effect may be due to the fact that the contribution of orbitals centered on aggregate silver atoms to LUMO is small and reaches only 40% at 12

TABLE VII

CALCULATIONS FOR Ag_2 ON AgBr

Geometry of AgBr	Total BE (eV)	Ag_2 charges	Charge on nearest Br of AgBr	Charge on nearest Ag of AgBr
		EH		
$(AgBr)_{14}$	9.49	+0.355, +0.236	−0.487	+0.378
$(AgBr)_8$	8.87	+0.361, +0.242	−0.485	+0.373
		CNDO		
$(AgBr)_6$	7.11	+0.332, +0.246	−0.681	+0.387
$(AgBr)_8$	8.01	+0.278, +0.166	−0.611	+0.389

TABLE VIII

EH CALCULATED DATA

Number of Ag	Type I BE/atom (eV)	HOMO (eV)	LUMO (eV)	Average Ag charge	Type II BE/atom (eV)	HOMO (eV)	LUMO (eV)	Average Ag charge
0	—	10.22	9.71	—	—	10.22	9.71	—
1	4.27	9.92	9.92	+.20	4.10	9.81	9.81	+.26
2	4.89	10.03	9.00	+.24	4.44	9.76	8.75	+.30
3	4.40	8.98	8.98	+.20	4.10	8.97	8.97	+.27
4	4.65	9.38	9.14	+.19	4.38	9.07	8.51	+.25
5	—		—		4.18	8.69	8.69	+.21
6	—		—		4.21	8.87	8.26	+.16
7	—		—		4.58	8.27	8.27	+.17
8	3.83	9.28	8.25	+.18	4.24	8.99	8.20	+.13

Number of Ag	Type III BE/atom (eV)	HOMO (eV)	LUMO (eV)	Average Ag charge
0	—	11.67	9.98	—
1	3.20	10.16	10.16	+.70
2	3.36	10.32	8.61	+.63
3	2.87	8.86	8.86	+.59
4	2.79	9.32	8.55	+.46
5	2.62	8.56	8.56	+.50

atoms of Ag. The other contributions come from 5*s* orbitals of Ag which tend to delocalize electrons throughout the crystal.

The substrate controls the most stable geometry of silver aggregates largely through the Madelung effect. A right triangle of three silver atoms is found to be more stable than a triatomic straight chain. For four atoms a very stable geometric configuration results for a square array with one side of the square touching the crystal and the other side above it. This is more stable by 1.29 eV than the square array touching the crystal at four sites. These results and those on graphite (3*b*) violate the intuitive idea that the site of maximum reactivity can form the most bonds.

The energy of a single silver atom is lower when it is next to Ag lattice sites than when it is next to

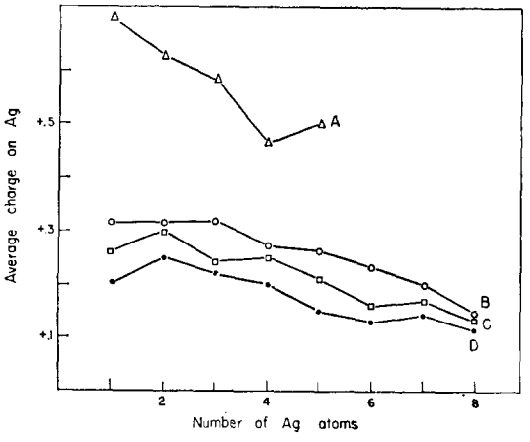

FIG. 8. Average charge on silver atoms vs number of silver atom sadded to $(AgBr)_{14}$ [EH]. Curve A: neutral system, type III; Curve B: system has one net positive charge, type II; Curve C: neutral system, type II; Curve D: system has one net negative charge, type II.

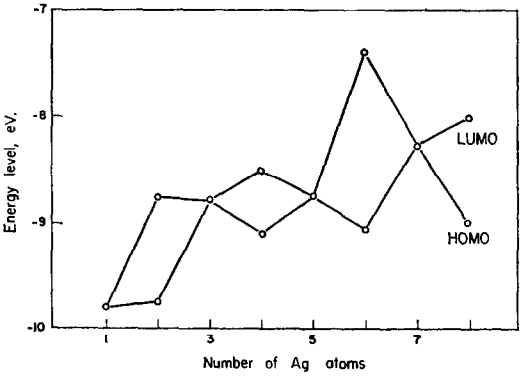

FIG. 9. Dependence of HOMO and LUMO on number of silver atoms added to $(AgBr)_8$ [EH].

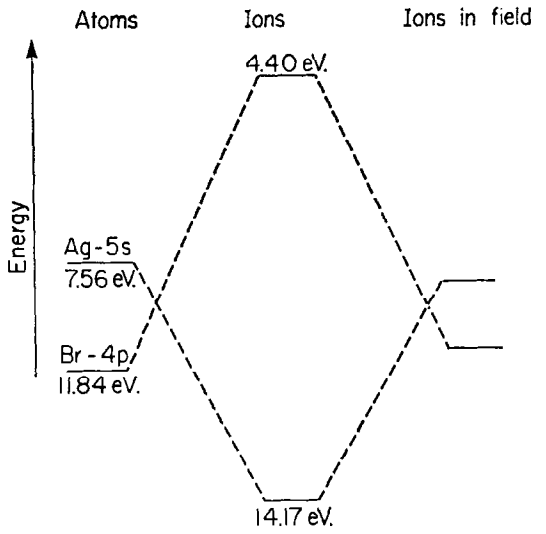

FIG. 10. Illustration of ionization and Madelung effects on atomic energy levels.

Br lattice sites. In addition, increasing the lattice positive charge in the neighborhood of the silver species stabilizes the silver species. The reasons for these effects are found by considering the Madelung and ionization potential effects on silver and bromine atoms. Figure 10 shows the energy levels of atoms, ions, and ions with a Madelung field. These general effects have been discussed (*7*). The effect of the Madelung field opposes the ionization effect because an electron is stabilized or destabilized depending upon whether the surrounding ions are positively or negatively charged, respectively. The net effect of both is to lower the 5*s* Ag levels and raise the 4*p* Br levels. When a silver atom adsorbs to a site on AgBr, the Madelung effect will act to raise or lower the atomic-orbital energy levels according to whether the immediately surrounding ions are negative or positive, respectively. Raising this level causes electrons to flow away from the adsorbing silver atom, and the converse holds. Thus, stabilization on adsorbing Ag results from lowering the orbital level, which can only be accomplished by positive ions. Therefore, low-energy, more stable silver aggregates can best form at positive sites such as dislocations or kinks.

The effect of model size in these EH calculations is minor. Calculations for Ag_2 on model 1 with and without plane I are summarized in Table VII. The electronic charges on Ag_2 and lattice ions show little effect of model size, although HOMO and LUMO appear to be shifted by ~0.4 eV.

Calculations for a planar AgBr geometry containing the same number of ions as Fig. 1 have been made. The result of defect structure is illustrated by this calculation. A significantly larger EA calculated by Eq. (13) is observed in the defect geometry (8.80 eV vs 7.23 eV for planar geometry). This effect can be understood by examining the wavefunction for LUMO. This wavefunction contains 5*s* Ag orbitals and halogen 4*p* orbitals for each direction in which there is a missing bond. The 4*p* orbitals have lower energy than 5*s* orbitals so the LUMO is more negative in the model with defect structure owing to the presence of more Br atoms on the surface. This surface state is an artifact of the model size because as the volume/surface ratio is increased, the state should contain decreasing contribution from halogen orbitals.

The effect of substrate structure on Ag particles is also examined by comparing calculations for a planar $(AgBr)_8$ geometry with calculations for the geometry of Fig 1. We find little effect on the binding energy of Ag particles to the substrate but a shift in energy levels, so that EA is larger for the small particles when they are located near the defect.

Discussion

The calculated data for aggregate energies can be applied to describe a mechanism of photolysis of AgBr. A small silver center produced by photolysis grows by attracting photoelectrons and mobile interstitial silver ions. The ability of the first process to occur is determined by the EA of the center relative to the EA of the rest of the crystal,

$$\Delta E_e = \mathrm{EA}_{(\mathrm{AgBr})\mathrm{Ag}_N} - \mathrm{EA}_{(\mathrm{AgBr})}. \qquad (16)$$

The energy released by the second process is given by

$$\Delta E_{\mathrm{Ag}^+} = E_{(\mathrm{AgBr})\mathrm{Ag}_{N+1}^+} - E_{(\mathrm{AgBr})\mathrm{Ag}_N} - \mathrm{BE}_{\mathrm{Ag}^+(\mathrm{AgBr})}. \qquad (17)$$

Table IX lists these values for small-size aggregates. Clearly, Ag_2 and Ag_4 centers in CNDO calculation cannot accept a photoelectron from the conduction band. As size increases, however, the larger even-size neutral aggregates can accept electrons, as the trend in LUMO shows in Table IX. The path of growth for the CNDO calculation which releases the most energy for each step is shown in Fig. 11. Previous mechanisms

TABLE IX

ENERGY RELEASED AT SILVER CENTER

Number of Ag atoms	E_c (eV)	$E_{Ag}+$ (eV)
	CNDO	
1	1.71	0.05
2	−0.56	0.90
3	1.62	0.61
4	−0.09	0.78
	EH—Defect model	
1	−0.96	1.10
2	1.84	0
3	2.38	0
4	1.75	0

(*25*, *26*) are different and did not include the alternating possibility for growth. Kinetic factors are not included in this mechanism; it must be remembered that these may exert a controlling influence on the reaction path.

The EH calculations agree with the CNDO results if a planar nondefect geometry is used. When the geometry of Fig. 1 containing defects serves as the lattice, electron-capture processes are favored at the expense of Ag^+ capture at the Ag center, as shown in Table IX. This leads to the alternative pathway in Fig. 12 and would explain a dependence of photochemistry on surface-defect structure.

The wavefunctions of the valence and conduction bands in AgBr are similar in EH and CNDO. The big difference is that LUMO lies close to the valence band edge in EH and far from the valence band edge in CNDO. Regardless of the true position, this level contains significant contribution from surface halogen orbitals. Thus, electrons occupying this level are delocalized over the positive and negative ions of the crystal.

A comparison of the calculation techniques with each other and with experimental bulk information leads to more confidence in the CNDO quantitative results. The AgBr band gap, EA, and cohesive energy correlate well with experiment. IP does not enjoy this position. The EH calculation does not agree nearly as well with the experimental, but this does not mean the relative Ag–AgBr interactions will be wrong. The general features of the semiconductor/metal interface are reproduced using CNDO or EH (type I or II). The noniterative EH calculations are inadequate for this problem.

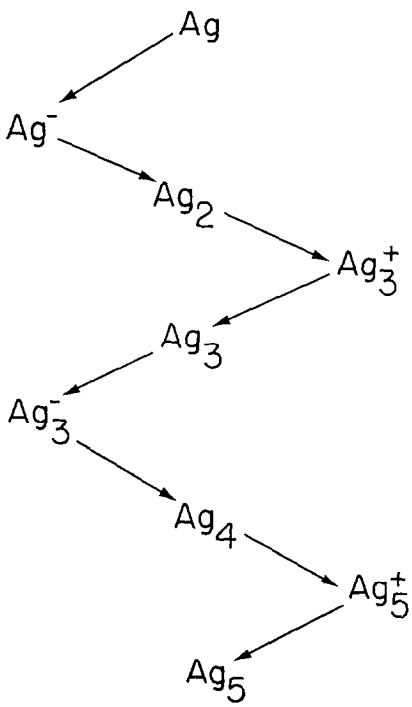

FIG. 11. Thermodynamic mechanism of Ag latent image formation on a plane surface [CNDO].

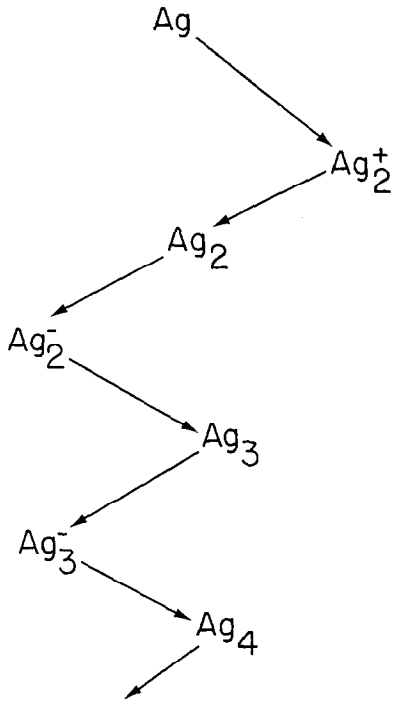

FIG. 12. Thermodynamic mechanism of Ag latent image formation at a defect site [EH].

Conclusions

Molecular orbital techniques provide an interpretation of Ag clusters on AgBr which is consistent with several experimental results. Absolute calculation of AgBr crystal parameters, such as BE/AgBr, EA, Req, and IP, by CNDO carry 10–20% error. Trends in the electron affinity and charge of the adsorbed Ag clusters indicate increasing stability with size as was observed for isolated Ag clusters.

Acknowledgments

I wish to thank J. F. Hamilton and H. E. Spencer of this Laboratory for many helpful conversations. Discussions with Dr. R. Hoffman of Cornell University provided grounds for beginning this program.

References

1. R. C. Baetzold, *J. Chem. Phys.* **55**, 4355 (1971).
2. (*a*) M. R. Hayns, *Phys. Rev. B.* **5**, 697 (1972); (*b*) D. Bramanti, M. Mancini, and A. Ranfagni, *Phys. Rev. B.* **3**, 3670 (1971).
3. (*a*) R. P. Messmer and G. C. Watkins, *Phys. Rev. Lett.* **25**, 656 (1970). (*b*) A. J. Bennett, B. McCarroll, and R. P. Messmer, *Phys. Rev. B* **3**, 1397 (1971); (*c*) A. J. Bennett, B. McCarroll, and R. P. Messmer, *Surface Sci.* **24**, 191 (1971); (*d*) D. J. M. Fassaert, V. Verbeek, and A. Van Der Avoird, *Surface Sci.* **29**, 501 (1972).
4. R. Hoffmann, *J. Chem. Phys.* **39**, 1397 (1963).
5. (*a*) J. A. Pople and G. A. Segal, *J. Chem. Phys.* **43**, 5136 (1965); **43**, S129 (1965); (*b*) J. A. Pople and G. A. Segal, *J. Chem. Phys.* **43**, S136 (1965); **44**, 3289 (1966); (*c*) D. P. Santry and G. A. Segal, *J. Chem. Phys.* **47**, 158 (1967).
6. (*a*) J. H. Corrington and L. C. Cusachs, *Spectrosc. Lett.* **1**, 67 (1968); (*b*) J. H. Corrington and L. Cusachs, *Int. J. Quantum Chem. Symp.* **3**, 207 (1969).
7. F. C. Brown, "The Physics of Solids," Benjamin, New York (1967).
8. F. A. Cotton, C. B. Harris, and J. J. Wise, *Inorg. Chem.* **6**, 909 (1967).
9. C. E. Moore, *Nat. Bur. Stand. Circ.* **1–3**, 467 (1949).
10. A. G. Gaydon, "Dissociation Energies," Chapman and Hall, London (1953).
11. R. S. Berry, C. W. Reiman, and G. N. Spokes, *J. Chem. Phys.* **37**, 2278 (1962).
12. E. Clementi and D. L. Raimondi, *J. Chem. Phys.* **38**, 2686 (1963).
13. R. S. Mulliken, *J. Chem. Phys.* **23**, 1833, 1841, 2238, 2343 (1955).
14. W. Jevons, "Report on Band Spectra of Diatomic Molecules," University Press, Cambridge (1932).
15. F. Bassani, R. S. Knox, and W. B. Fowler, *Phys. Rev. A* **137**, 1217 (1965).
16. B. L. Joesten and F. C. Brown, *Phys. Rev.* **148**, 919 (1966).
17. F. C. Brown, *J. Phys. Chem.* **66**, 2368 (1962).
18. L. C. Cusachs and J. H. Corrington, *in* "Sigma M.O. Theory" (O. Sinanoglu and K. Wiberg, Eds.), Yale University Press, New Haven, CT (1970).
19. R. S. Bauer, Technical Report 5218–3, Stanford Electronics Laboratory, Stanford, CA (1971).
20. N. J. Carrera, Ph.D. dissertation, University of Illinois (1970).
21. W. Gomes, *Trans. Faraday Soc.* **59**, 1648 (1963).
22. R. K. Ahrenkiel and R. S. VanHeyningen, *Phys. Rev.* **144**, 576 (1966).
23. P. Suptitz, *Z. Phys.* **153**, 174 (1958).
24. C. E. K. Mees and T. H. James, "The Theory of the Photographic Process," 3rd ed., Macmillan, New York (1966).
25. L. E. Brady and J. F. Hamilton, *J. Appl. Phys.* **37**, 2268 (1966).
26. J. W. Mitchell, *J. Phys. Chem.* **66**, 2359 (1962).